Neutron diffraction and ultrasonic studies of the helical implies/implied by paramagnetic phase transition in dysprosium and holmium

1995 J. Phys.: Condens. Matter 7 9863

(http://iopscience.iop.org/0953-8984/7/50/020)

J. Phys.: Condens. Matter 7 (1995) 9863–9882. Printed in the UK

Neutron diffraction and ultrasonic studies of the helical ↔ paramagnetic phase transition in dysprosium and holmium

Paul de V Du Plessis†, A M Venter‡ and G H F Brits‡

† Physics Department, University of the Witwatersrand, PO WITS 2050, Johannesburg, South Africa

‡ Atomic Energy Corporation of SA (Ltd), PO Box 582, Pretoria, South Africa

Received 5 September 1995

Abstract. Neutron diffraction measurements on high-purity Dy and Ho crystals indicate no discontinuity in the order parameter at T_N, and no hysteresis in the value of T_N within 0.05 K between consecutive cooling and heating runs. This finding is also reflected by the results of ultrasonic velocity and attenuation measurements, thus corrobrating the continuous nature of the phase transition. Integrated neutron diffraction measurements near T_N yield $\beta = 0.38 \pm 0.02$ for Dy and $\beta = 0.39 \pm 0.02$ for Ho in agreement with renormalization group predictions ($\beta = 0.39$) of Mukamel, Krinsky and Bak. Neutron intensities in the paramagnetic region do not adhere to a conventional $t_+^{-\gamma}$ dependence over the complete temperature regime. A possible description for the region near T_N with a 2D-planar spin model is indicated. The critical velocity change Δv_{33} of Ho near T_N is discussed.

1. Introduction

The nature of the planar helical ↔ paramagnetic phase transition in dysprosium and holmium has been the focus of considerable theoretical and experimental interest. Using a renormalization group approach Mukamel, Krinsky and Bak (MKB) co-cluded, on the basis of the existence of a stable fixed-point Hamiltonian, that the phase transition is continuous [1, 2]. By considering a symmetric $O(n)$ model with the number of order parameter components $n = 4$ and for dimensionality $d = 3$ by setting $\epsilon = 1$ in series expansions calculated to order ϵ^2, values for the critical exponents ν and η were found. Furthermore, using the scaling laws they obtained critical exponent values $\beta = 0.39$, $\gamma = 1.39$, $\alpha = -0.17$ and $\nu = 0.70$. These characterize the sublattice magnetization $M \sim [(T_N - T)/T_N]^{\beta} = t_-^{\beta}$, the susceptibility $\chi \sim [(T - T_N)/T_N]^{-\gamma} = t_+^{-\gamma}$, the specific heat anomaly near T_N, *viz.* $\Delta C \sim t_\pm^{-\alpha_\pm}$, and the divergence of fluctuating magnetic domains near T_N through the correlation length $\xi \sim t_+^{-\nu}$. Kawamura [3, 4] proposed the existence of a new universality class for these helical magnets by considering a generalized Landau–Ginzburg–Wilson Hamiltonian with $n = 2$ and $d = 3$. This model predicts values of $\beta = 0.25$, $\gamma = 1.10$, $\alpha = 0.4$ and $\nu = 0.53$ which are significantly different from the MKB predictions. Barak and Walker [5] argued, on the other hand, that the initial Hamiltonian that describes these systems does not lie in the domain of the stable fixed point and consequently the criterion [6] for a second-order phase transition is not fully met. Thus these systems are expected to be driven first-order by critical fluctuations. Finally, Azaria *et al* [7] question the existence of a new universality class in this case and propose the existence of a tricritical point in their phase diagram. Many experiments on the helical ↔ paramagnetic phase

0953-8984/95/509863+20$19.50

transition in Dy and Ho have been analysed and interpreted on the assumption that the transition is of second order. Values thus obtained for the critical exponents β, ν, γ, α_+ and α_- are given in table 1 for Dy [8–15] and table 2 for Ho [10, 11, 15–24].

Table 1. Critical exponents of dysprosium.

Value of exponent	Ref.	Reduced temperature range	Method	Details about sample
β=0.335	[8]	$0.003 \lesssim t_- \lesssim 0.3$	Mössbauer	Single crystal
$\beta = 0.39^{+0.04}_{-0.02}$	[9]	$0.003 \lesssim t_- \lesssim 0.2$	Neutrons	Single crystal (Metals Research Ltd) Purity 99.99 wt% RRR[a] ~ 13
β=0.39 ±0.01	[10]	$0.0011 \lesssim t_- \lesssim 0.0086$	Neutrons	Single crystal previously used by [9]
$\nu = 0.57 \pm 0.05$	[11]	$0.008 \lesssim t_+ \lesssim 0.1$	Neutrons	Single crystal
γ=1.05 ± 0.07	[11]	$0.008 \lesssim t_+ \lesssim 0.1$	Neutrons	Single crystal
$\alpha_+ = -\alpha_- = 0.02 \pm 0.01$	[12]	$0.005 \lesssim t_\pm \lesssim 0.32$	ac calorimetry	Single crystal
$\alpha_+ = \alpha_- = 0.18 \pm 0.02$	[12]	$0.0005 \lesssim t_\pm \lesssim 0.005$	ac calorimetry	Single crystal
$\alpha_- = -0.25 \pm 0.2$	[13]	$0.005 \lesssim t_- \lesssim 0.092$	Calorimetry	Sample purified by vacuum sublimation, [a] RRR = 82
$\alpha_+ = 0.12^{+0.22}_{-0.12}$	[13]	$0.015 \lesssim t_+ \lesssim 0.3$	Calorimetry	
$\alpha_- = -0.205^{+0.07}_{-0.09}$	[13]	$0.0094 \lesssim t_- \lesssim 0.082$	Calorimetry	Sample purified by vacuum sublimation [a] RRR = 200
$\alpha_+ = 0.17^{+0.1}_{-0.06}$	[13]	$0.0081 \lesssim t_+ \lesssim 0.12$	Calorimetry	
$\alpha_+ = 0.49 \pm 0.29$	[13]	$0.056 \lesssim t_+ \lesssim 0.39$	Calorimetry	
$\alpha_+ = \alpha_- = 0.16 \pm 0.01$	[14][b]	$0.004 \lesssim t_- \lesssim 0.025$	Adiabatic continuous heating calorimetry	Single crystal Ames Laboratory 99.98 wt%
$\alpha_+ = \alpha_- = 0.33 \pm 0.01$	[14][c]	$0.004 \lesssim t_- \lesssim 0.025$		
$\alpha_+ = \alpha_- = 0.24 \pm 0.02$	[14][d]	$0.005 \lesssim t_+ \lesssim 0.08$		
$\alpha_+ = \alpha_- = 0.46 \pm 0.02$	[14][e]	$0.005 \lesssim t_+ \lesssim 0.08$		
$\eta_+ = 1.26 \pm 0.1$	[15]	$0.003 \lesssim t \lesssim 0.1$	Ultrasonics	Single crystal (c axis propagation)

[a] RRR indicates the ratio of resistivities at room temperature and 4.2 K and is a measure of sample purity.
[b–e] Analyses to obtain $\alpha_\pm$ from their specific heat data by [12] and [13] were carried out using a pure power-law function. In the case of [14], results indicated by b and c refer to use of a function that includes correction to scaling terms. Results b and d furthermore refer to keeping the background contribution to the specific heat continuous through T_N while c and e allow for a discontinuous background in specific heat at T_N.

The critical resistivity ρ near the magnetic phase transition is characterized by $\mathrm{d}\rho(T)/\mathrm{d}(T) = B_\pm t^{-\lambda_\pm}$. For ferromagnets it is usually accepted that $\rho(T)$ has a magnetic energy-like dependence near T_C, i.e. $\lambda = \alpha$. The situation in antiferromagnets and helically ordered rare earths is less clear due to the existence of superzone gaps, the complications of crossover from critical to mean field behaviour and possible effects of the Fermi-surface geometry [25, 26, 27]. It seems that any value of λ between α and the mean-field value of 0.5 can be obtained depending on the $t_\pm$ range over which the measurements were analysed. For this reason results from the large number of resistivity studies in the literature are not included in tables 1 and 2. It should nevertheless be mentioned than an detailed analysis [27] of the high-resolution measurements of Rao *et al* [28] on Dy gave $\alpha_+ = \alpha_- = -0.04 \pm 0.005$ for $3 \times 10^{-4} \lesssim t \lesssim 3 \times 10^{-2}$. The critical softening of the velocity of longitudinal sound waves in the crystal near T_N may be described by $\Delta v/v_o \sim t_\pm^{-\zeta_\pm}$ and the attenuation anomaly by $\Delta\alpha \sim \omega^2 t_\pm^{-\eta_\pm}$. Values for the critical exponents ζ_+ and η_+ are given in tables 1 and 2

Table 2. Critical exponents of holmium.

Value of exponent	Reference	Reduced temperature range	Method	Details about sample
$\beta = 0.39^{+0.04}_{-0.03}$	[16]	$0.01 \lesssim t_- \lesssim 0.3$	Neutrons	Single crystal, 10 mm long, 1 mm ϕ
$\beta = 0.39 \pm 0.03$	[10]	$0.01 \lesssim t_- \lesssim 0.1$	Neutrons	Single crystal: 99.98 wt% Metal crystals [a] RRR ~ 13
$\beta = 0.3 \pm 0.1$	[17, 18]	$0.001 \lesssim t_- \lesssim 0.0076$	Neutrons	Single crystal
$\beta = 0.37 \pm 0.1$	[17, 18]	$0.001 \lesssim t_- \lesssim 0.0076$	x-rays	Single crystal
$\beta = 0.327$	[19]	$0.002 \lesssim t_- \lesssim 0.1$	Neutrons	Single crystal
$\beta = 0.41 \pm 0.04$	[20]	$t_- \lesssim 0.24$	x-rays	Single crystal
$\beta = 0.39 \pm 0.04$	[20]	Asymptotic limit $T \to T_N$		
$\nu = 0.57 \pm 0.04$	[11]	$0.002 \lesssim t_+ \lesssim 0.2$	Neutrons	Single crystal
$\gamma = 1.14 \pm 0.10$	[11]	$0.002 \lesssim t_+ \lesssim 0.2$	Neutrons	Single crystal
$\nu = 0.54 \pm 0.04$	[18]	$0.001 \lesssim t_+ \lesssim 0.1$	Neutrons	Single crystal
$\gamma = 1.24 \pm 0.15$	[18]	$0.005 \lesssim t_+ \lesssim 0.08$	Neutrons	Single crystal
$\nu = 1.0 \pm 0.3$	[18] [b]	$0.001 \lesssim t_+ \lesssim 0.005$	Neutrons	Single crystal
$\gamma = 4.5$	[18] [b]	$0.001 \lesssim t_+ \lesssim 0.005$	Neutrons	Single crystal
$\nu = 1.0$	[18] [b]	$0.0005 \lesssim t_+ \lesssim 0.01$	X-rays	Single crystal
$\gamma = 3.4$	[18] [b]	$0.0006 \lesssim t_+ \lesssim 0.01$	X-rays	Single crystal
$\alpha_+ = \alpha_- = 0.08 \pm 0.03$	[21] [c]	$0.000\,16 \lesssim t_- \lesssim 0.0063$	Adiabatic	Single crystal
$\alpha_+ = \alpha_- = 0.26 \pm 0.01$	[21] [d]	$0.000\,16 \lesssim t_- \lesssim 0.0063$	continuous	Ames Laboratory
$\alpha_+ = \alpha_- = 0.34 \pm 0.01$	[21] [e]	$0.000\,12 \lesssim t_+ \lesssim 0.0013$	heating	99.99 wt%
$\alpha_+ = \alpha_- = 0.27 \pm 0.02$	[21] [f]	$0.000\,12 \lesssim t_+ \lesssim 0.0013$	calorimetry	purity
$\alpha_+ = \alpha_- = 0.10 \pm 0.02$	[22, 23] [c]	$0.002 \lesssim t_\pm \lesssim 0.05$	Heat pulse	Single crystal as
$\alpha_+ = \alpha_- = 0.22 \pm 0.02$	[22, 23] [f]		calorimetry	used in [11]
$\zeta_+ = 0.21 \pm 0.03$	[24]	$0.01 \lesssim t_+ \lesssim 0.2$	ultrasonics (c axis propagation)	Single crystal
$\eta_+ = 1.0 \pm 0.1$	[15]	$0.0003 \lesssim t_+ \lesssim 0.1$	ultrasonics (c axis propagation)	Single crystal

[a] RRR indicates the ratio of resistivities at room temperature and 4.2 K and is a measure of sample purity.
[b] These higher values of ν and γ refer to the new longer-length-scale (narrow-component) scattering recently observed [17, 18].
[c–f] Analyses to obtain $\alpha_\pm$ from their specific heat data by [21, 22, 23] were carried out using a power-law analysis (indicated by c and d) or using a function that includes correction to scaling terms (indicated by e and f). The results c and e furthermore refer to keeping the background contribution to the specific heat continuous through T_N, while d and f allow a discontinuous background in specific heat at T_N.

[15, 24]. One also notes that a logarithmic dependence has been indicated for $\Delta v/v_0$ [15].

A central question pertains to the order of the helical ↔ paramagnetic phase transition. In previous work [10] we addressed this problem by precise measurements of the sublattice magnetization (with neutrons) and of ultrasonic velocity and attenuation from which the continuous nature of the phase transition and absence of hysteresis effects at T_N for Dy

and Ho crystals have been concluded. These crystals, from Metals Research and Metals Crystals respectively, were of moderate purity with residual resistance ratios (RRR) of $R_{300\ K}/R_{4.2\ K} \sim 13$. Several studies claim the existence of a first-order transition. Tindall *et al* [29] observed a strain discontinuity at T_N of magnitude $\Delta l/l = 30 \times 10^{-6}$ along the a axis of a Ho crystal, but later measurements by the same group on a different crystal did not confirm this result [30]. Zochowski *et al* [31] observed a 0.2 K hysteresis in the value of T_N from the results of c axis strain measurements on a high-purity Dy crystal. One cautions against accepting this as proof of a first-order transition since the hysteresis was inferred from an extrapolation of non-equilibrium data recorded at two different heating rates and one fixed cooling rate. White [32] found no length discontinuity along either c or a axes of a Ho crystal. Using a high-resolution differential microcalorimeter, Åström and Benedictson [33] observed a small hysteresis of 0.3 ± 0.1 K in T_N for a high-purity Dy crystal between heating and cooling measurements taken at a rate of temperature change of 1 mK s^{-1}. They also observed a hysteresis of 0.4 ± 0.1 K for a high-purity Ho crystal [34], and a sharp energy peak at T_N for both elements. These results were interpreted as evidence of a weak first-order transition. This is in contrast to the specific heat studies [12–14, 21–23] referred to in tables 1 and 2 which treated the transition as continuous. Jayasuriya *et al* [21] observed no latent heat at T_N for a Ho crystal heated at a slow rate of 0.4 mK s^{-1} with constant power input.

Extracting the appropriate critical exponents from experimental data proves to be difficult. Since the RKKY interaction is long ranged [35], the critical region is expected to be small for these rare-earth magnets [36] and has been estimated for Dy as $t \lesssim 10^{-2}$ [27]. The regions of validity for the numerical fits from which exponents were deduced are indicated in tables 1 and 2 in reduced temperature units t_- or t_+. In many cases these exceed $t \sim 10^{-2}$ and some of the observed discrepancies may presumably be resolved by finding the $t_\pm \to 0$ limits in the analyses. In neutron scattering studies of the order parameter, extinction effects [37] are important and this could influence the observed values of β. The effect of sample purity is believed to be important [38], but the only systematic studies pertaining to critical exponents of the helical rare earths seem to be by Amitin *et al* on Dy [13].

It is evident from tables 1 and 2 that the observed values of β mostly favour the MKB prediction ($\beta = 0.39$) and are in disagreement with the value of $\beta = 0.25$ indicated by Kawamura. On the other hand, the observed ν and γ values [11, 18] are in closer agreement with the predictions of Kawamura than with that of MKB. There is fair agreement between the specific heat results for Ho observed by Jayasuriya *et al* [21] and Wang *et al* [22, 23], but a significant difference in α values is observed depending on whether the specific heat background at T_N is taken as continuous or discontinuous [22]. In the case of Dy a large spread in α values has been observed. The values of α given in tables 1 and 2 are not considered to favour any particular model describing the critical behaviour. Amitin *et al* [13] found for Dy that in a small temperature region just above T_N the magnetic specific heat cannot be described by the expected critical behaviour for a second-order phase transition or by assuming a first-order character for the transition. They rather suggest the existence of a vortex spin structure and the applicability of a two-dimensional XY model as described by Kosterlitz and Thouless [39, 40].

An important recent development has been the observation of two length scales in the magnetic critical fluctuations of holmium [17, 18] and terbium [41, 42] by high-spatial-resolution x-ray and neutron scattering in a temperature region close to T_N ($t_+ \lesssim 0.01$). Experimentally, the critical scattering in this temperature region is composed of both a broad and a narrow component and can be described by the sum of a Lorentzian plus a

squared Lorentzian. Fitting the resulting half-widths for the two components to a power-law form, HWHM $\sim t_+^{\nu}$, it is found that the narrow component is characterized by a value $\nu = 1.0$ while the broad component does not adhere to a power-law dependence in this region. Well above T_N only the broad component (i.e. the shorter of the two length scales) is observed in the neutron scattering results and the HWHM conforms to a power law with $\nu = 0.54$. A difference in the γ exponents is furthermore deduced for the narrow and broad components (table 2) and it has been suggested that the broad component ($\gamma = 1.24$, $\nu = 0.54$) corresponds with the conventional critical fluctuations. The narrow component (i.e. the longer length scale) has been shown in the case of Tb to originate mostly in a thin near-surface volume or skin of the crystal [41, 42] and is thought to originate in random strain fields associated with defects at the surface of the sample [18]. It has recently been proposed [43] that long-range random strains associated with edge dislocations introduced during sample polishing in the surface of the Ho or Tb crystals are responsible for a crossover to a 'disordered' fixed point with a corresponding change in critical exponents [44] as is indeed observed for the narrow component [17, 18, 41, 42]. For the high-resolution and weakly penetrating x-rays the narrow component is preferentially observed in both transverse and longitudinal scans for Ho. In order to observe both components with neutrons it was necessary to perform transverse scans through the $(0, 0, \delta)$ satellite since this represents a high-spatial-resolution measurement. The longitudinal $(0, 0, \delta)$ scans are of such appreciably lower resolution in the neutron case that the narrow component cannot be resolved.

2. The scope of the investigation

In view of the uncertainty of the nature of the helical ↔ paramagnetic transition we extend our previous neutron diffraction and ultrasonic studies on less pure Dy and Ho crystals to measurements on high-purity Dy (RRR = 68) and Ho (RRR $\approx$ 100) crystals. As indicated in section 3, on the experimental details of our investigation, considerable care was taken to ensure thermal equilibrium conditions and temperature stability during measurements. Simultaneous neutron scattering and ultrasonic measurements were performed to search for discontinuous behaviour or for hysteresis in T_N from the results of consecutive cooling and heating runs (section 4). Within the resolution of our experiments the helical ↔ paramagnetic transition was observed as continuous and without hysteresis for both Dy and Ho crystals. Results of integrated neutron diffraction measurements of the $(0, 0, 2 - \delta)$ satellite are given in section 5 for both materials, in order to determine the critical exponent β. The possible influences of critical scattering and extinction effects, as well as the dependence of β on the range of t_- values used, are considered. It is observed that the paramagnetic neutron scattering does not follow the $t_+^{-\gamma}$ dependence expected for critical scattering and it is indicated in section 5 that the neutron intensities may be fitted to the predicted behaviour of a 2D-planar spin model [40]. Results on the ultrasonic critical behaviour of Ho are given in section 6. A discussion of our new results in the context of the existing literature is presented in section 7.

3. Experimental details

Neutron scattering experiments were performed using a two-axis spectrometer at the Safari-I reactor facility of the AEC of South Africa. A germanium(311) monochromator crystal was used to select 1.402 Å neutrons for measurements on the Dy crystal and germanium(111)

for obtaining a beam of wavelength 1.072 Å for measurements on Ho. Both peak and integrated intensity measurements for the $(0, 0, 2 - \delta)$ satellite were performed. Peak intensity measurements, where both the crystal and counter are kept stationary at the Bragg position, were used to qualitatively study the behaviour of the magnetization in Dy close to T_N. This mode of operation results in improved counting statistics which is required for a highly absorbing material like Dy (μ = 18 cm^{-1} [37]) to limit the experiment to reasonable lengths of time. However, for determining β of Dy, and for all experiments on Ho, integrated intensity measurements of the $(0, 0, 2 - \delta)$ satellite were performed using $(\omega, 2\theta)$ scans [37] with step sizes of 0.036° in ω through the Bragg position. The c and a axes of the crystals were aligned in the scattering plane by employing either a κ–ϕ or a Huber four-circle goniometer for the low-temperature measurements described below. Ultrasonic velocity and attenuation measurements were made during the same run using a MATEC 7700 system. A pulse–echo overlap technique was used for the velocity measurements and the attenuation was obtained by comparing the peak heights of two selected echoes with a logarithmic voltmeter. Valpey Fisher X-Cut overtone polished quartz transducers of fundamental frequency 10 MHz were used to propagate a longitudinal wave along the c axis of either the Dy or Ho crystal. The transducer was stuck to the flat surface of the cube-shaped crystal using Araldite standard epoxy. Cooling of the Dy crystal was achieved with a nitrogen gas flow cryostat of our own design [10] while an Air Products and Chemicals model DE-202-OSP two-stage closed-cycle helium Displex refrigerator was used for studies on the Ho crystal. For neutron scattering measurements a Lake Shore DTC-500 temperature controller, using a silicon diode sensor, was employed. Application of an RF signal had a detrimental influence on the output from the Si diode sensor and hence a THOR S3010 controller, employing a Au–0.07 at.% Fe versus chromel-P thermocouple, was used in all ultrasonic measurements. The crystal was secured with thin aluminium wire and a minimum of GE 7031 varnish to an aluminium sample stalk which was screwed against an indium seal on to the copper cold finger of the cryostat. This ensured unimpeded thermal expansion of the crystal. Crystals were enclosed in a helium-filled aluminium hood filled with helium exchange gas.

Sample temperatures were measured with two Au + 0.07 at.% Fe versus chromel-P thermocouples secured on two opposite faces of the crystal. An ice triple-point cell provided a stable reference temperature during experimental runs which often took up to five days. The data accumulation time for the neutron diffraction measurements at each selected temperature point took up to 60 min, and 30 min was allowed for temperature stabilization between temperature changes to ensure that thermal equilibrium has been reached. Temperatures were controlled to a relative stability of better than ±0.02 K.

One Dy crystal and two Ho crystals (designated Ho1 and Ho2) were supplied by the Materials Preparation Center, Ames. The crystals were all shaped as cubes of approximate sizes 6 mm × 6 mm × 6 mm. The principal a, b and c axes were perpendicular to the cube faces. We measured an RRR value of 68 for the Dy crystal and note that an RRR value of 100 has been specified by the suppliers for the Ho crystals. In the case of the Dy crystal it was necessary for the ultrasonic work to prepare new parallel surfaces by spark-erosion planing and subsequent etching in a 50% nitric acid:50% lactic acid solution. The Ho crystals were initially studied as received, but in the course of the project crystal Ho1 was cut using spark erosion to provide a disc and various pillar-shaped samples for certain measurements.

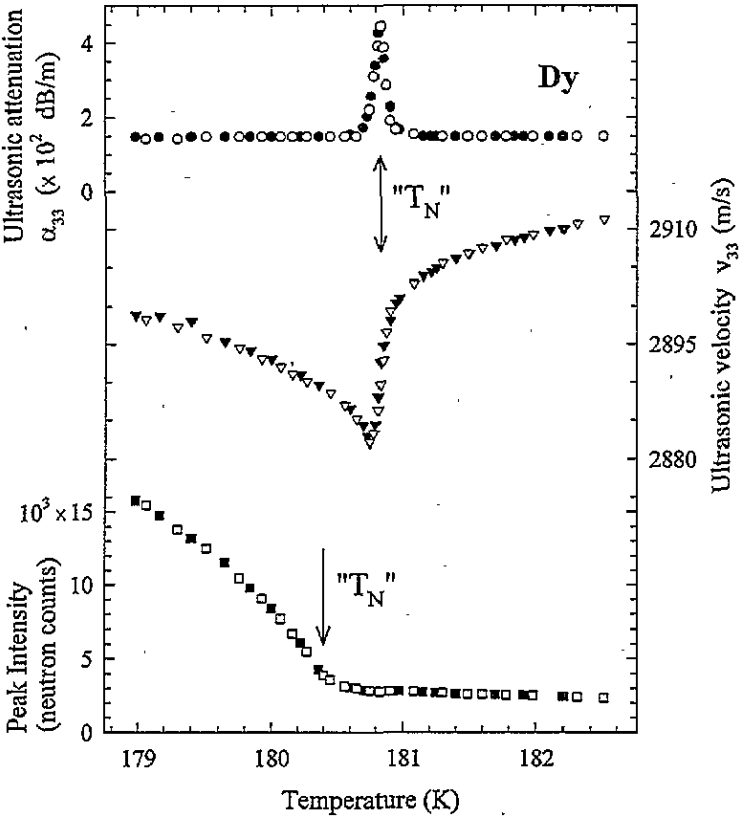

Figure 1. Simultaneously measured ultrasonic velocity v_{33} and attenuation α_{33}, and peak scattered neutron intensity versus temperature for single-crystal Dy. The longitudinal ultrasonic wave was propagated along the c axis and neutrons probed the $(0, 0, 2 - \delta)$ satellite. Open symbols indicate measurements taken during the cooling part of the experiment and closed symbols refer to the subsequent heating run.

4. Characterizing the phase transition

4.1. Experiments on dysprosium

Detailed measurements were performed to search for discontinuous behaviour or hysteresis in the helical ↔ paramagnetic transition of the high-purity Dy crystal. Results of measurements of neutron peak intensities of the $(0, 0, 2 - \delta)$ magnetic satellite and of ultrasonic velocity and attenuation for longitudinal waves propagated along the c axis of the crystal during the same run are indicated in figure 1. Open symbols indicate results obtained in the cooling part of the experiment, which was followed by a heating run (closed symbols). This convention will be used throughout the paper to indicate cooling or heating modes of the runs. It is evident that no discontinuity in the order parameter is observed from the neutron scattering results and that within 0.05 K no hysteresis is evident from any of the three types of measurement. The superior quality of the present Dy crystal compared to the sample studied earlier [10] is evident by comparing the attenuation peaks which were in both cases measured at 10 MHz. It is found that the full-width at half-maximum (FWHM) for the Ames sample is 0.09 K while the FWHM for the less-pure sample is 0.46 K. We have also performed measurements in which the crystal was cycled five times between 170

and 220 K after the first cooling run before a second set of data points was taken during a cooling run. This experiment was done in order to investigate a reported large change of 13 K in T_N when cycling a Dy crystal through T_N [45]. Such an effect would make the study of critical properties meaningless but, in a way similar to previous results on the less-pure Dy crystal [46], we observed no dependence of T_N on thermal cycling for the purer Dy crystal [47]. We note that a systematic temperature error occurred in our previous experiment resulting in temperatures reported in [10] and [47] being 1.5 K too low. This error has been corrected for in all figures pertaining to Dy in the present paper. An unexpected result is evident from figure 1. Associating the position of the attenuation peak and the inflection point in the velocity curve with the critical temperature, a value of $T_N = 80.83$ K is obtained. This is 0.43 K higher than the value of T_N indicated by neutron scattering, as is evident from figure 1. Dy has a high neutron absorption coefficient and hence neutrons scattered off the (0, 0, 2) face of the cubic-shaped sample (i.e. in a reflection mode) only probe a thin skin of the crystal. The experiment was repeated by rotating the crystal through 180° in order that neutrons may be scattered off the $(0, 0, \bar{2})$ cube face. The same difference between T_N observed from neutron and ultrasonic measurements was found, and the phenomenon is called a ΔT_N effect. A frequency dependence of T_N, as indicated in the ultrasonic measurements, could give a trivial explanation of the effect. However, comparative measurements at 10, 30 and 50 MHz showed no frequency dependence of T_N. Finally, from simultaneous measurements of the anomaly of the elastic constant C_{44} and neutron scattering, the ΔT_N anomaly was also observed. A possible origin of the ΔT_N effect may be from defects in the surface of the material, for instance, introduced during cutting or electropolishing of the crystal. Also, gas absorption of, for example, H_2 takes place in lanthanides which has the effect of shifting the phase transition to lower temperatures (see [48] for results on erbium). Since the neutrons only probe the near-surface regions while the ultrasonic measurements probe the bulk crystal, it is possible that the neutron measurements indicate a lower T_N which results from surface damage of the sample. The ΔT_N effect may therefore be interpreted to be of a similar origin to that of the narrow component in the critical neutron or x-ray scattering, *viz.* as a surface phenomenon [41, 42] possibly originating from the stress fields associated with dislocations in the crystal [43]. It is noted that in measurements on the less-pure Dy sample [10] no ΔT_N effect was observed, presumably indicating either less surface damage or a smaller influence of damage on T_N for this sample.

4.2. Experiments on holmium

A number of experiments were performed which investigated the order of the phase transition and hysteresis effects, as well as a possible ΔT_N effect in Ho at the same time. The thermal neutron absorption coefficient is smaller ($\mu = 1.6$ cm^{-1} [37]) for Ho than for Dy and consequently the neutrons can penetrate deeper into the crystal. In the search for a ΔT_N anomaly the neutron sampling volume for crystal Ho1 was controlled by selecting different sample regions by attaching 1 mm thick cadmium foil ($\mu = 121$ cm^{-1}) to the sample. Measuring the integrated intensity down to temperatures of 1.8 K below T_N for these different crystal regions, selected by appropriate Cd masking, also formed part of investigating the extinction for this crystal. The following Cd-masking arrangements were employed: (A) all cube faces were masked except the front (0, 0, 2) face from which neutrons were scattered; (B) the front and back (0, 0, 2) cube faces were masked, as well as strips of 1 mm wide on the cube sides as indicated in figure 2; (C) the whole crystal was exposed; (D) only a small triangular pillar was exposed as illustrated in figure 3. The

continuous nature of the phase transition as observed on the Ho1 crystal is evident from figure 2. Furthermore, although significant hysteresis in scattered neutron intensities in the helically ordered region was previously observed for crystals Ho1 and Ho2 [49] when cooling the crystal only 4 K below T_N, the data within 2 K of T_N are seen to be hysteresis free. Hence in determining the critical exponent β (see section 5), the experiment was executed in a temperature region not extending further than 2 K below T_N. The ultrasonic results also confirm the essential absence of hysteresis in the location of T_N. It is also noted from figure 2 that no ΔT_N effect is evident for the Ho crystal. These preceeding results were also corroborated by measurements using masking arrangement A.

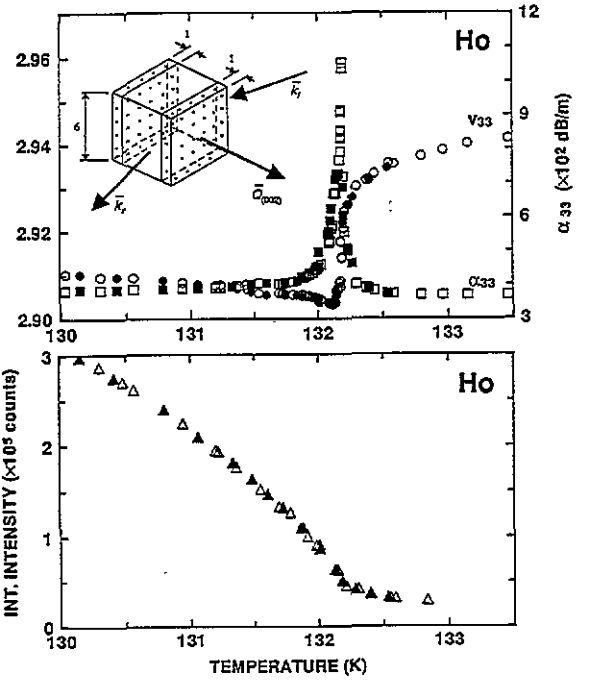

Figure 2. Simultaneously measured ultrasonic velocity v_{33} and attenuation α_{33} and integrated neutron intensity versus temperature for the Ho1 crystal. The longitudinal ultrasonic wave was propagated along the c axis and neutrons probed the $(0, 0, 2-\delta)$ satellite while passing through the bulk of the crystal on account of the Cd-masking arrangement indicated. Open symbols refer to cooling and closed symbols refer to the subsequent heating run.

An empirical evaluation of the influence of extinction was made by comparing the magnetic integrated intensity observed from the $(0, 0, 2-\delta)$ satellite between T_N and 130 K using the Cd-masking arrangements as indicated. The intensity observed for the triangular pillar was taken as a standard and data for the other three arrangements A, B and C were plotted against that obtained for D, as shown in figure 3. Each point represents a measurement taken at the same temperature and monitored for the same count limit. Curve B, which indicates a situation with neutrons passing through the sample with equal path lengths of approximately 6.8 mm, indicates a clear deviation from linearity at lower temperatures which should be ascribed to extinction. Curve C shows only a small deviation for the higher-intensity lower-temperature points relative to the expected linear dependence of an 'extinction free' experiment. This indicates that the longer path lengths contribute less to the scattered intensity for the unmasked crystal. For the situation where neutrons

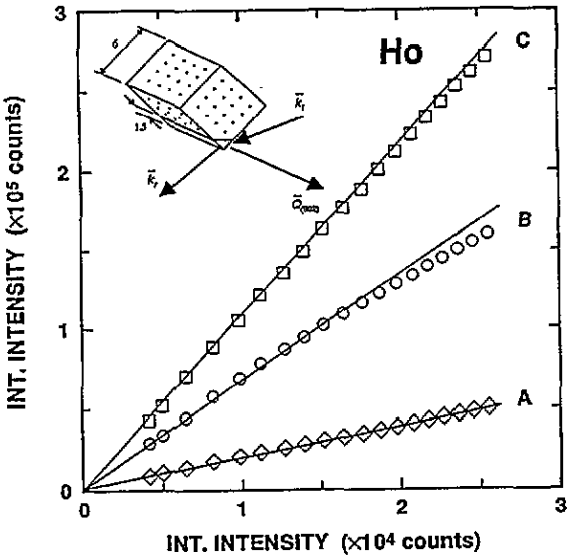

Figure 3. Plots of the integrated intensities measured on the Ho1 crystal for Cd-masking arrangements A, B and C versus the integrated intensity of the triangular pillar obtained by masking arrangement D (see main text for a discussion).

are scattered only from the front surface in a reflection mode, a linear dependence through the origin is satisfied, thereby indicating minimal extinction (curve A). A suitable crystal for a neutron diffraction study of the critical behaviour near T_N was selected as a trade-off between limiting the neutron path length through the crystal to reduce extinction and providing enough crystal volume to enhance the total scattered intensity. To this end and taking cognizance of the results of figure 3, a slab of thickness 2.5 mm containing the (b, c) plane was spark erosion cut from crystal Ho1 (cutting speed 6 on a Servomet machine). This crystal, designated as Ho1S, was used for measurements in transmission of the $(0, 0, 2-\delta)$ neutron intensities as described in section 5.

5. Critical exponent β measured with neutron diffraction

Integrated neutron intensities measured for the $(0, 0, 2-\delta)$ satellite on crystal Ho1S in transmission, at regulated temperatures during a cooling run, are depicted in figure 4 after subtracting a background component. The presence of substantial intensity at the satellite position for temperatures well above T_N is noted. Analysis of the neutron intensity I near the phase transition is usually performed [10] in terms of the following equation

$$\begin{aligned} I &= I_M + I_{C_+} + I_{C_-} \\ &= Bt_-^{2\beta} + C_+t_+^{-\gamma} + C_-t_-^{-\gamma}. \end{aligned} \tag{1}$$

The magnetic part $I_M \propto M^2$ contributes only below T_N while I_{C_+} and I_{C_-} denote contributions due to the coherent critical scattering from dynamically fluctuating domains above and below T_N, respectively. From the scaling-law hypothesis γ is considered to be the same above and below T_N. The amplitudes C_+ and C_- of the scattering differ, but are related though Schofield's parametric representation of the equation of state [50]

$$\frac{C_+}{C_-} = \frac{\gamma}{\beta}\left[\frac{(1-2\beta)\gamma}{2(\gamma-1)\beta}\right]^{\gamma-1}. \tag{2}$$

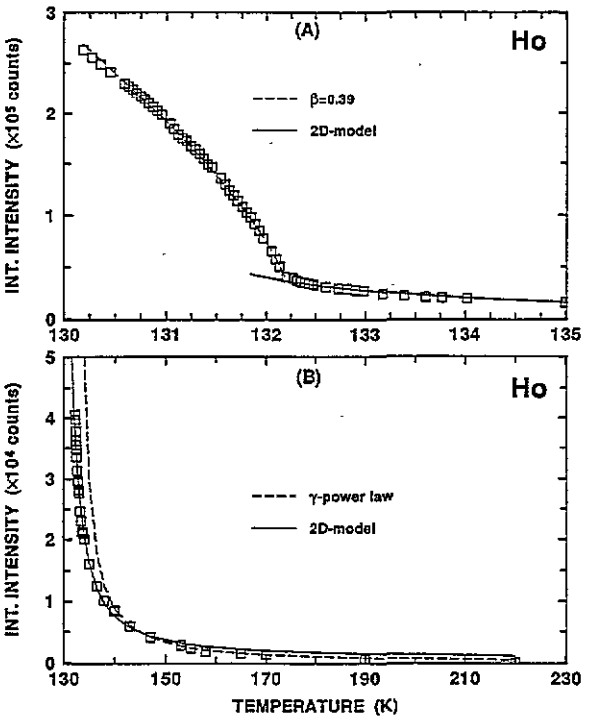

Figure 4. Integrated intensity for the $(0, 0, 2-\delta)$ reflection versus temperature for Ho1S. In (A) fits to a $t_-^{2\beta}$ dependence of the spontaneous magnetization in the ordered region and to a 2D-planar spin model in the paramagnetic region ($I \sim e^{D\epsilon^{-1/2}}$) are indicated. In (B) fits to the persistent intensity observed in the paramagnetic region are indicated as discussed in the text.

In our usual procedure [10] optimum values for γ, T_N and C_+ are obtained by iterative least-squares analysis of the paramagnetic data. Hence, using equation (2) the critical scattering contribution I_{C_-} is calculated as a correction to the data below T_N, thus yielding the spontaneous magnetization which is analysed to find β. From figure 5 it follows that the integrated intensities observed in the paramagnetic region do not follow the expected power-law behaviour, $I_{C_+} = C_+ t_+^{-\gamma}$, with a unique value of γ. In the region close to T_N, 132.5 K $\lesssim T \lesssim$ 135.0 K, the behaviour is described by $\gamma = 0.33 \pm 0.05$, whereas for 140 K $\lesssim T \lesssim$ 170 K a value $\gamma = 1.21 \pm 0.05$ is observed. The value $\gamma = 0.33$ observed near T_N clearly does not correspond to any scaling-law expectations. Our value of $\gamma = 1.21$ observed at higher temperatures agrees with the value $\gamma = 1.14 \pm 0.10$ reported by [11] over a similar temperature region and with the value $\gamma = 1.24 \pm 0.15$ associated with the shorter length scale of the critical scattering from Ho [18]. It is noteworthy that whereas the broad component deviates from the $\gamma = 1.24$ power law in the latter case (figure 11 in [18]) at $t_+ \sim 4 \times 10^{-3}$, the deviation from the high-temperature power law takes place at $t_+ \sim 3 \times 10^{-2}$ in figure 5 for our low-spatial-resolution $(0, 0, 2-\delta)$ measurements. Another possible description for the neutron intensity above T_N is hence considered. It is indicated in figure 4 that below ~140 K the intensity may be well represented by

$$I = C\, e^{D\epsilon^{-\frac{1}{2}}} \tag{3}$$

where $\epsilon = (T - T_C)/T_C$ and T_C is a critical temperature. This type of dependence is reminiscent of that deduced by Kosterlitz [40] to describe the critical behaviour in the limit

of approaching T_C from above for a 2D-planar spin model. Similar agreement with the prediction of the 2D-planar model was observed by Betsuyaku [51] at temperatures above the weak first-order phase transition in chromium, where it was suggested that the paramagnetic intensity originates from clusters of remnant magnetic ordering. With increasing temperature the sizes of these clusters diminish and this subsequently leads to the decrease in the coherent intensity at the satellite positions.

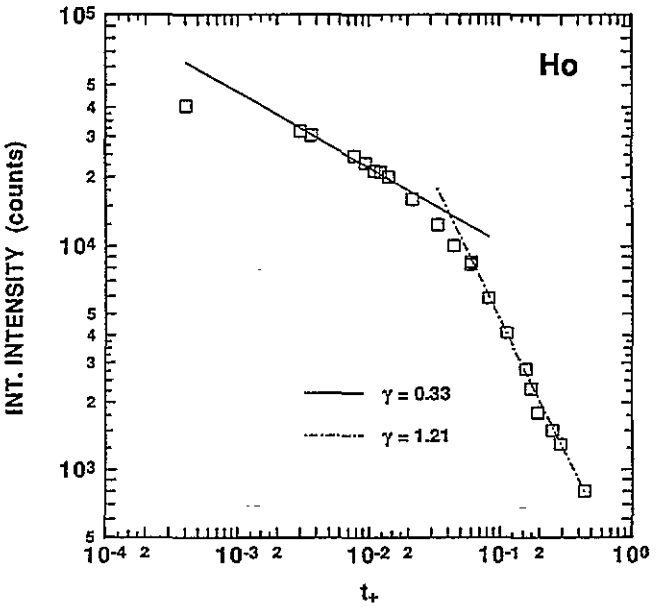

Figure 5. A double logarithmic plot of the $(0, 0, 2-\delta)$ integrated neutron intensity against t_+ for crystal Ho1S with $T_N = 132.15$ K. A γ power law can be fitted in two regions, but with different slopes as indicated.

It is clear from figure 5 that although it seems to be appropriate to describe the high-temperature data in terms of a $t_+^{-\gamma}$ dependence, such a description is not valid at all near T_N. It would consequently be inappropriate to correct the critical scattering by extrapolating the $t_+^{-\gamma}$ dependence and use it to calculate a correction $C_-t_-^{-\gamma}$ to the data points below T_N. It is rather recognized that the dominant intensity is described well by equation 3 and the intensity at $T_N = 132.15$ K, *viz.* $I' = 37\,800$ has rather been used as a constant background for all data shown below T_N in figure 5. Fitting $I - I'$ to an $I_M = Bt_-^{2\beta}$ dependence gives an excellent fit with the parameters given in table 3. The deviation between the fit for the spontaneous magnetization and the data points for temperatures below 130.5 K may be ascribed to either a breakdown in scaling or as a result of extinction. During a process whereby successively lower temperature points were removed one after the other in the least-squares analysis, the β values remained within the limits specified in table 3.

Integrated neutron diffraction intensities of the $(0, 0, 2-\delta)$ satellite after subtraction of the background intensity are indicated in figures 6 and 7 for Dy. In these measurements the bulk of the Dy crystal was screened from neutrons with a 1 mm thick cadmium sheet such that only two small triangular pillars were exposed to the neutron beam (similar to the screening arrangement for Ho shown in figure 3). It is indicated in figure 6 that the relationship $I_{C_+} = C_+t_+^{-\gamma}$ is not uniquely obeyed for the high-quality Dy single crystal either. Two distinct slopes $\gamma = 0.42 \pm 0.05$ near T_N and $\gamma = 1.34 \pm 0.05$ at higher

Table 3. Fit parameters for the helical ↔ paramagnetic phase transition in Ho and Dy as studied by neutron scattering.

Fit parameters for holmium			
	$T < T_N$ $I_M = B t_-^{2\beta}$		$T > T_N$ $I = C e^{D\epsilon^{-\frac{1}{2}}}$
Reduced temperature range of fit	$1.9 \times 10^{-4} \lesssim t_- \lesssim 1.57 \times 10^{-2}$	Temperature range of fit	132.20 K $\lesssim T \lesssim$ 190.00 K
B	6.00×10^6	C	356
β	0.39 ± 0.02	D	1.01 ± 0.05
T_N	132.15 ± 0.02 K	T_C	126.3 ± 0.1 K
Fit parameters for dysprosium			
	$T < T_N$ $I_M = B t_-^{2\beta}$		$T > T_N$ $I = C e^{D\epsilon^{-\frac{1}{2}}}$
Reduced temperature range of fit	$3.3 \times 10^{-4} \lesssim t_- \lesssim 8.3 \times 10^{-3}$	Temperature range of fit	180.90 K $\lesssim T \lesssim$ 197.97 K
B	7.26×10^5	C	1030
β	0.38 ± 0.02	D	1.03 ± 0.05
T_N	180.65 ± 0.02 K	T_C	157.7 ± 0.1 K

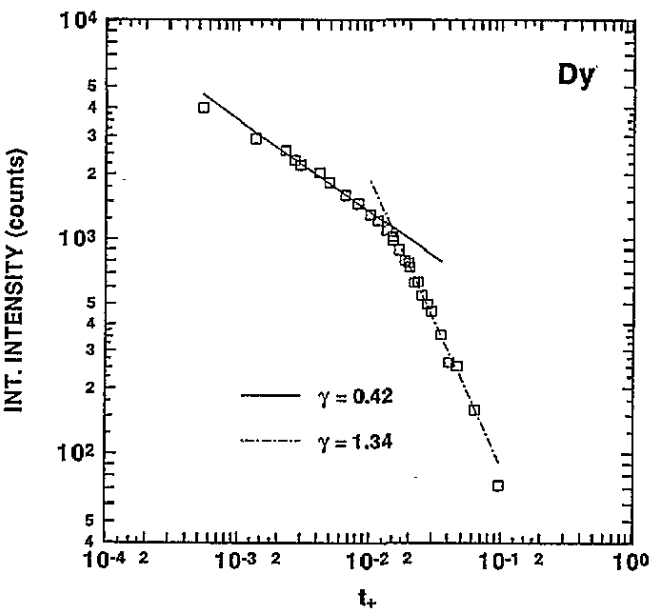

Figure 6. A double logarithmic plot of the $(0, 0, 2 - \delta)$ integrated neutron intensity versus t_+ for Dy with $T_N = 180.65$ K. A γ power law can be fitted in the two regions with different slopes as indicated.

temperatures can be deduced from a log I versus log t_+ graph, as shown in figure 6. In a way similar to the results obtained for the Ho crystal, the first value of γ falls outside the scaling-law predictions, whereas although the second value does comply to the scaling law it only describes the paramagnetic behaviour at least 3 K above T_N. This behaviour is in distinct contrast to the results previously obtained for a less pure Dy crystal which indicated

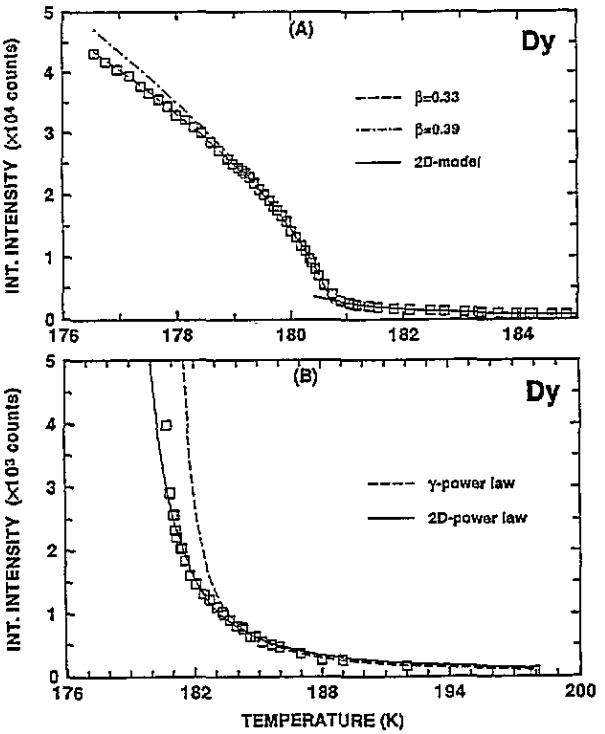

Figure 7. Integrated intensity for the $(0, 0, 2-\delta)$ reflection versus temperature for Dy. In (A) fits to a $t_-^{2\beta}$ dependence of the spontaneous magnetization in the ordered region and to a 2D-planar spin model in the paramagnetic region ($I \sim e^{D\epsilon^{-1/2}}$) are indicated. In (B) fits to the persistent intensity observed in the paramagnetic region are indicated as discussed in the text.

a single value of $\gamma = 1.2$ for $0.003 \lesssim t_+ \lesssim 0.025$ [10].

Using reasoning analogous to that given for Ho, an analysis of the neutron diffraction data of Dy has been performed by assuming that the critical correction below T_N is negligible and that the paramagnetic intensity just above T_N is described by the 2D-planar model. The paramagnetic behaviour is approximated by an exponential function, equation (3), indicated in figure 7 by a solid line and with fit parameters given in table 3. Using the intensity at T_N, $I' = 3050$, a least-squares analysis of $I - I'$ to an $I_M = Bt_-^{2\beta}$ dependence gives the fit displayed by a broken line in figure 7 and with fit parameters given in table 3. The spontaneous magnetization is adequately described by $\beta = 0.38$ over a temperature range extending 1.2 K below $T_N = 180.65$ K, and with $\beta = 0.33$ when including data points as low as 4 K below T_N. The decrease in the value of β when lower-temperature points are included in the analysis may be ascribed to either a break down in scaling or extinction effects. As figure 7(B) shows, the 2D-planar model fits quite well to the paramagnetic data points ranging from T_N to about 184 K, but deviates at higher temperatures where the γ power-law fit renders better correspondence to the experimental points.

6. The ultrasonic critical behaviour of holmium

From figures 1 and 2 it is evident that the longitudinal velocity and attenuation along the c axis clearly indicate the helical $\leftrightarrow$ paramagnetic phase transition in Dy and Ho. A longitudinal sound wave propagating within a magnetic crystal produces an oscillation

of the distance between neighbouring spins, thereby modifying the exchange interaction $J(R_{ij})$ between two spins i and j. This leads to an interaction between the sound wave and the spins and gives rise to the attenuation of sound in magnetic materials. As the magnetic phase transition is approached the rapid growth in fluctuating magnetic domains gives rise to a peak in the sound attenuation at T_N. The coupling between the spin system and the acoustic wave can be of a single-ion magnetostrictive nature or due to exchange magnetostriction [15]. Since it is observed that the shear attenuation along symmetry directions shows a negligible anomaly at the transition it is inferred that the coupling is of an exchange magnetostrictive nature [15]. Bennett [52] showed that in magnetic systems in which the interaction of the acoustic longitudinal phonons with the magnetic moments is of an exchange magnetostrictive origin, a negative frequency shift results on approaching the phase transition. The maximum frequency shift occurs at the transition temperature and is governed by a power-law dependence, giving

$$\Delta v_{33}/v_0 = -\omega^0 t^{-\zeta}. \tag{4}$$

Here v_0 is the unperturbed velocity, ω^0 is a frequency-independent constant and the exponent ζ is predicted to have values in the region $0 \lesssim \zeta \lesssim 0.66$. The upper bound is dictated by scaling laws whereas the lower bound is obtained from heuristic corrections made by Bennett [53] to allow for the overestimation of the critical fluctuations in the four-spin correlation function [54]. Furthermore, $\Delta v_{33}/v_0$ has been found for Dy to be proportional to the magnetic part of the specific heat [55] in which case ζ may be equated to the specific heat critical exponent α. An investigation of the critical velocity change at the helical ↔ paramagnetic phase transition was undertaken by propagating 10 MHz longitudinal sound waves along the c axis of the Ho2 crystal. Simultaneous velocity and attenuation measurements were taken, with the temperature stable to within ± 0.02 K, at temperatures extending from 300 K to 125 K with small temperature graduations in the region close to T_N. Corrections for the variation of the acoustical path length using known thermal expansion results [56] were made and found to account for a variation in v_{33} of less than 0.2% at 128 K relative to the 300 K reference. Values of v_{33} are depicted in figure 8. To extract Δv_{33} from the experimental results the 'normal' temperature dependence of the velocity in the absence of the magnetic phase transition must be known. Ideally, one could obtain this by using the non-magnetic rare-earth metal lutetium as a reference compound. Unfortunately, it is observed that the C_{33} elastic constant of Lu has an anomalous temperature dependence at low temperatures [57]. Use was therefore made of a linear extrapolation of the higher-temperature $v_{33}(T)$ data down to T_N in order to extract Δv_{33} values (see figure 8). The validity of such an extrapolation seems reasonable since the Debye temperature θ_D is 188 K for Ho [58]. It is observed that the elastic constants of most materials have a linear negative temperature dependence down to at least $\frac{1}{2}\theta_D$, before they eventually approach 0 K with zero slope [59, 60]. This is borne out, in particular, for the C_{33} elastic constant of several non-magnetic hexagonal metals (magnesium, zinc, cadmium and beryllium) [60, 61].

The critical exponent ζ in equation (4) was extracted by a least-squares-fit analysis of double-log plots of $(-\Delta v_{33}/v_0)$ versus t_+, as indicated in figure 9 (A and B). An iteration procedure was followed where T_N and the temperature range of the fit were treated as variables. The best fits obtained are for both $T_N = 131.95$ K and $T_N = 132.0$ K with $0.002 \lesssim t_+ \lesssim 0.032$. Both these linear regressions yield $r^2 = 0.998$ and an exponent $\zeta = 0.23 \pm 0.03$. The fit for $T_N = 132.0$ K is shown in figure 9(A) and it is evident that for $t_+ > 0.032$ equation (4) is not followed. The aforementioned values of T_N found in the fit procedure are visibly lower than the minimum in v_{33} or the peak value of the attenuation (see figure 2). Using the value $T_N = 132.15$ K found from the peak in attenuation leads to

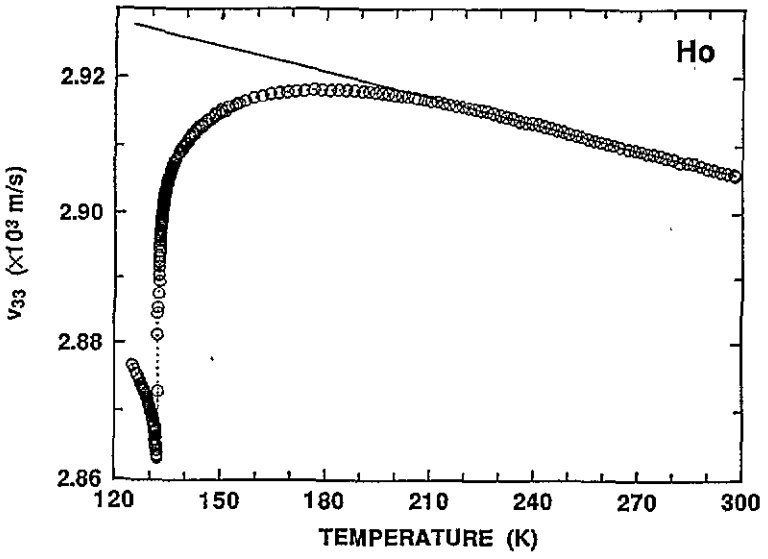

Figure 8. Longitudinal velocity v_{33} versus temperature for ultrasonic waves propagated along the c axis of crystal Ho2. The solid line represents the 'normal' temperature dependence expected for a non-magnetic crystal in the temperature region of interest.

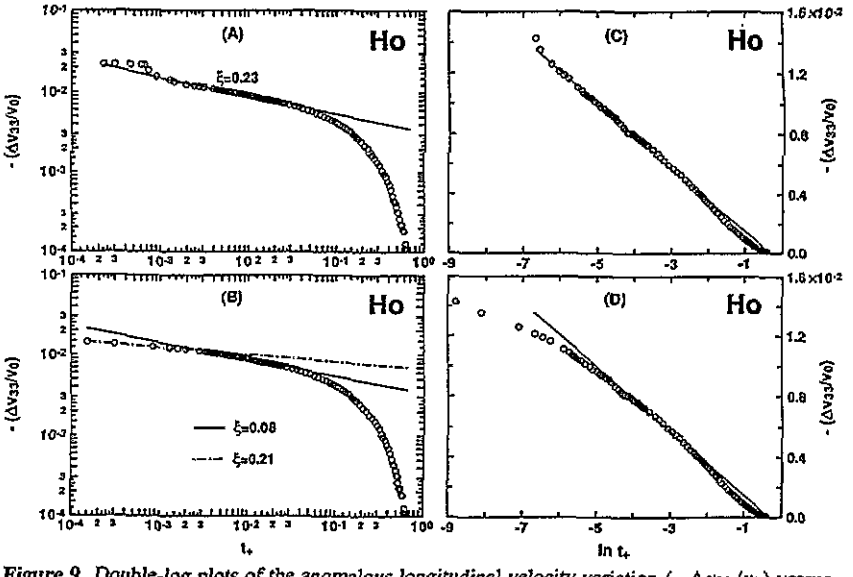

Figure 9. Double-log plots of the anomalous longitudinal velocity variation $(-\Delta v_{33}/v_0)$ *versus* t_+ are given in (A) for $T_N = 132.0$ K and in (B) for $T_N = 132.15$ K. Plots of $(-\Delta v_{33}/v_0)$ versus ln t_+ are indicated in (C) for $T_N = 132.0$ K and in (D) for $T_N = 132.15$ K. The significance of these presentations and T_N iterations is discussed in section 6.

the $(-\Delta v_{33}/v_0)$ against t_+ dependence indicated in figure 9(B). A value of $\xi = 0.21 \pm 0.03$ is obtained for $0.0033 \lesssim t_+ \lesssim 0.032$ and with $r^2 = 0.993$. Closer to T_N a further power-law dependence is found with $\zeta = 0.08 \pm 0.03$, *viz.* for $1.5 \times 10^{-4} \lesssim t_+ \lesssim 3.3 \times 10^{-3}$, and with $r^2 = 0.985$. A weaker temperature dependence for the critical longitudinal velocity change

on approaching T_N from the paramagnetic phase has been indicated for Tb, Dy and Ho by Lüthi *et al* [15]

$$\Delta v_{33}/v_0 = -\omega^0 \ln t_+. \tag{5}$$

Plots of $(-\Delta v_{33}/v_0)$ against $\ln t_+$ are indicated in figure 9(C) for $T_N = 132.0$ K and in figure 9(D) for $T_N = 132.15$ K. An excellent fit ($r^2 = 0.999$) is obtained in figure 9(C) for $0.002 \lesssim t_+ \lesssim 0.1$ which appreciably extends the region of validity of the fit at high temperatures beyond that observed when fitting against equation (4). When $T_N = 132.15$ K is used in figure 9(D) it is observed that the region in which a satisfactory fit is obtained is reduced near T_N.

7. Discussion

The nature of the helical ↔ paramagnetic phase transition in these rare earths, the validity of scaling and universality and the possibility of crossover effects are discussed in this section with special reference to our results. Our neutron scattering measurements on Dy and Ho crystals, taken with fine temperature resolution, show no evidence of a discontinuity in order parameter at T_N. Ultrasonic velocity and attenuation results, as well as neutron scattering measurements taken in cooling runs followed by subsequent heating runs, also showed no hysteresis in the value of T_N within 0.05 K. These results strongly suggest the second-order nature of the phase transition and consequently allow for the extraction of critical exponents and consideration of the validity of scaling and universality for these systems. One should nevertheless be aware that measurements with improved resolution on higher-purity crystals may ultimately observe a (presumably small) first-order transition for these materials. The case history of chromium is a good example of how the first-order nature of the magnetic transition in that element has only eventually been observed by measurements on high-purity and nearly-strain-free crystals [62]. One does note that a difference in T_N observed from neutron and ultrasonic measurements was found for Dy (but not for Ho). This is thought to be a surface effect as discussed in section 4.

The two length scales that are observed for Ho in high-spatial-resolution x-ray and neutron critical scattering studies [17, 18] cannot be resolved in our low-spatial-resolution $(0, 0, 2 - \delta)$ integrated neutron measurements on Ho and Dy reported in section 5. The narrow component has been shown to originate in a skin of ~0.2 mm thick in the case of a Tb crystal [41, 42]. If a skin thickness of the same order of magnitude applies to our Ho and Dy crystals, an appreciable contribution to the measured intensity due to the narrow component is to be expected in the experiments of section 5. Our integrated neutron intensity measurements for both Ho and Dy show that the scaling-law description obtained reasonable γ values at higher temperatures but breaks down below $t_+ \sim 4 \times 10^{-2}$ for Ho and $t_+ \sim 10^{-2}$ for Dy. In section 5 we showed that the paramagnetic intensity in an initial temperature region above T_N (see figures 4 and 7) has a temperature dependence expected for the behaviour of a 2D-planar spin model [40]. This paramagnetic intensity is thought to originate from clusters of remnant magnetic ordering [51]. It seems to us that defects in both skin and bulk may, due to their associated strain fields, lead to such remnant magnetism. Hence the value of t_+ where the high-temperature scaling law breaks down in our studies, need not correspond with the t_+ value where the narrow component emerges in the neutron experiments of Thurston *et al* [17, 18]. Indeed for Ho the latter value is about an order of magnitude less than the former.

Values of the critical exponent β of both Ho and Dy are obtained from experiments with short neutron path-lengths and performed over a limited temperature interval below

T_N. Hence, the results should not be significantly influenced by extinction. The observed values of $\beta = 0.39 \pm 0.02$ for Ho and $\beta = 0.38 \pm 0.02$ for Dy are in agreement with the prediction of MKB ($\beta = 0.39$) rather than with the expectation of Kawamura ($\beta = 0.25$). Reference to table 2 indicates that such a value of β now seems to be well established for measurements taken in a temperature interval close to T_N. Tang *et al* [63] recently used the pulsed neutron beam from the ISIS spallation source (Rutherford Appleton Laboratory) for Laue diffraction studies of Ho and Tb. A determination of the temperature dependence of the sublattice magnetization of Tb was performed for $t_- \lesssim 0.035$ for several magnetic satellites. An average value of $\beta = 0.23 \pm 0.04$ was obtained, which corresponds to the prediction of Kawamura. This new result for Tb seems to indicate a lack of universality of the helically ordered rare earths. One is somewhat concerned with the large value of integrated intensity observed near T_N when compared to the intensity for $t_- \sim 0.035$ (see figure 11 of [63]). This could indicate either that a large background intensity has not been subtracted or that the data do not extend up to T_N. It is also noted that the results for various reflections range from $\beta = 0.15$ to $\beta = 0.27$. In an earlier investigation [9] we obtained $\beta = 0.32$, also with a large scatter (+0.06, −0.04), from neutron diffraction measurements from the $(0, 0, 2 \pm \delta)$ satellites studied in five different temperature runs. These studies were complicated by the persistence of ferromagnetic order into the helical region and the existence of a broad tail of scattering above T_N which could not be ascribed to critical scattering. In view of the preceding considerations it may be premature to conclude a non-universal behaviour for the helical rare earths based on the results for Tb.

The ultrasonic critical velocity $\Delta v_{33}/v_0$ (section 6) shows some evidence for a crossover of the power-law dependence from an exponent $\zeta = 0.23 \pm 0.03$ at higher temperatures to a value of $\zeta = 0.08 \pm 0.03$ below $t_+ \sim 3.3 \times 10^{-3}$. The former value is in good agreement with a value of $\zeta = 0.21 \pm 0.03$ observed by Goncharov *et al* for $t \gtrsim 0.01$ and also with some of the values for the specific heat critical exponent α_+ given in table 2. This also confirms the proportionality between $\Delta v_{33}/v_0$ and the magnetic part of the specific heat for Ho, as previously observed for Dy [55].

The effect of long-range dipolar interactions on the critical behaviour of ferro- and antiferromagnets has been treated in a series of papers by Aharony and Fisher [64, 65, 66, 67] using the renormalization group approach. A crossover to a dipolar dominated region for $t_+ \lesssim t_d = \hat{g}^{1/\phi}$ is expected. The strength of the dipolar coupling relative to the exchange is indicated by $\hat{g}$ and ϕ is the crossover index. Considering Dy as a XY ferromagnet with $\epsilon = 1$, $n = 2$ and $\phi = 1.32$, Lederman and Salamon [12] expected crossover at $t_d \sim 0.005$. Their experimental heat capacity results for single-crystal Dy indeed indicated a crossover from an outer region with $\alpha_+ = \alpha_- = -0.02 \pm 0.01$ to an inner region with $\alpha_+ = \alpha_- = +0.18 \pm 0.08$ at a temperature in agreement with the theoretical expectations. Jayasuriya *et al* [14] re-examined the data by Lederman and Salamon and found that some of their fitting parameters for data in the inner region are in error and state that their claim [12] of a crossover at $|t_d| \sim 0.005$ is incorrect. The plethora of other $\alpha_\pm$ values given in tables 1 and 2 for Dy and Ho are mostly an order of magnitude bigger than the $\alpha = 0.02$ found by Lederman and Salomon for the outer region $t_\pm \gtrsim 0.005$ of Dy. Furthermore it is evident that the resulting values of α depend to a considerable measure on such basic assumptions as whether the constraint $\alpha_+ = \alpha_-$ is to be used and whether the background specific heat should be taken as continuous or discontinuous through T_N in the analysis.

The hyperscaling relationship $\alpha + 2\beta + \gamma = 2$ [68] is now used in conjunction with our values of β, and with γ as given by [11] and [18] used to predict the α exponent. For Dy, using $\beta = 0.38 \pm 0.02$ and $\gamma = 1.05 \pm 0.07$ [11], this leads to $\alpha = 0.19 \pm 0.11$. For Ho, using $\beta = 0.39 \pm 0.02$, one finds $\alpha = 0.08 \pm 0.14$ when using $\gamma = 1.14 \pm 0.10$ [11] and

$\alpha = -0.02 \pm 0.19$ when using $\gamma = 1.24 \pm 0.15$ [18]. The calculated values of α do not support the predictions of either MKB ($\alpha = -0.17$) or Kawamura ($\alpha = 0.4$). A clear need for further experiments, especially to determine α and γ, is evident. Future work on the critical properties of the rare earths should furthermore take cognizance of the influence of defects on the critical behaviour and attempt to determine exponents that are characteristic of the bulk.

Acknowledgments

The support of the Atomic Energy Corporation of South Africa, in providing equipment, running costs and neutron beam time, is greatly appreciated. Professor E Fawcett is thanked for the loan of the single crystals used in this study and for numerous discussions in the initial stages of this project, especially on the possible role of dislocations in the ΔT_N effect.

References

[1] Mukamel D and Krinsky S 1976 *Phys. Rev.* B **13** 5065
[2] Bak P and Mukamel D 1976 *Phys. Rev.* B **13** 5086
[3] Kawamura H 1988 *J. Appl. Phys.* **63** 3086
[4] Kawamura H 1988 *Phys. Rev.* B **38** 4916
[5] Barak Z and Walker M B 1982 *Phys. Rev.* B **25** 1969
[6] Wilson K G and Kogut J 1974 *Phys. Rep.* C **12** 75
[7] Azaria P, Delamotte B and Jolicoeur T 1990 *Phys. Rev. Lett.* **64** 3175
[8] Loh E, Chien C L and Walker J C 1974 *Phys. Lett.* **49A** 357
[9] Du Plessis P de V, Van Doorn C F and Van Delden D C 1983 *J. Magn. Magn. Mater.* **40** 91
[10] Brits G H F and Du Plessis P de V 1988 *J. Phys. F: Met. Phys.* **18** 2659
[11] Gaulin B D, Hagen M and Child H R 1988 *J. Physique Coll.* **49** C8 327
[12] Lederman F L and Salomon M B 1974 *Solid State Commun.* **15** 1373.
[13] Amitin E B, Bessergenev V G and Kovalevskaya Yu A 1983 *Sov. Phys.–JETP* **57** 117
[14] Jayasuriya K D, Campbell S J and Stewart A M 1985 *Phys. Rev.* B **31** 6032
[15] Lüthi B, Moran T J and Pollina R J 1970 *J. Phys. Chem. Solids* **31** 1741
[16] Eckert J and Shirane G 1976 *Solid State Commun.* **19** 911
[17] Thurston T R, Helgesen G, Gibbs D, Hill J P, Gaulin B D and Shirane G 1993 *Phys. Rev. Lett.* **70** 3151
[18] Thurston T R, Helgesen G, Hill J P, Gibbs G, Gaulin B D and Simpson P J 1994 *Phys. Rev.* B **49** 15 730
[19] Tindall D A, Adams C P, Steinitz M O and Holden T M 1994 *J. Appl. Phys.* **75** 6318
[20] Helgesen G, Hill J P, Thurston T R, Gibbs D, Kwo J and Hong M 1994 *Phys. Rev.* B **50** 2990
[21] Jayasuriya K D, Campbell S J and Stewart A M 1985 *J. Phys. F: Met. Phys.* **15** 225
[22] Wang J, Belanger D P and Gaulin B D 1991 *Phys. Rev. Lett.* **66** 3195
[23] Wang J, Belanger D P and Gaulin BD 1992 *J. Magn. Magn. Mater.* **117** 356
[24] Goncharov K V, Maĭtseva I V and Savitskii E M 1972 *Sov. Phys.–Solid State* **13** 3125
[25] Alexander S, Helman J S and Balberg I 1976 *Phys. Rev.* B **13** 304
[26] Richard T G and Geldart D J W 1977 *Phys. Rev.* B **15** 1502
[27] Balberg I and Maman A 1979 *Physica* B **96** 54
[28] Rao K V, Rapp Ö, Johanneson Ch, Geldart D J W and Richard T G 1975 *J. Phys. C: Solid State Phys.* **8** 2135
[29] Tindall D A, Steinitz M O and Plumer M L 1977 *J. Phys. F: Met. Phys.* **7** L263
[30] Steinitz M O, Kahrizi M and Tindall D A 1987 *Phys. Rev.* B **36** 783
[31] Zochowski S W, Tindall D A, Kahrizi M, Genosser J and Steinitz M O 1986 *J. Magn. Magn. Mater.* **54–7** 707
[32] White G K 1989 *J. Phys.: Condens. Matter* **1** 6987
[33] Åström H U and Benediktson G 1988 *J. Phys. F: Met. Phys.* **18** 2113
[34] Åström H U and Benediktson G 1985 *5th Gen. Conf. EPS Condensed Matter Division Berlin* Abstract, quoted by [33]
[35] Coqblin B 1977 *The Electronic Structure of Rare-Earth Metals and Alloys: the Magnetic Heavy Rare-Earths* (New York: Academic)

[36] Collins M F 1989 *Magnetic Critical Scattering* (New York: Oxford University Press)
[37] Bacon G E 1975 *Neutron Diffraction* (Oxford: Clarendon)
[38] Cadieu F J and Douglass D H Jr 1968 *Phys. Rev. Lett.* **21** 680
[39] Kosterlitz J M and Thouless D J 1974 *J. Phys. C: Solid State Phys.* **6** 1181
[40] Kosterlitz J M 1974 *J. Phys. C: Solid State Phys.* 7 1046
[41] Gehring P M, Hirota K, Majkrzak C F and Shirane G 1993 *Phys. Rev. Lett.* **71** 1087
[42] Hirota K, Shirane G, Gehring P M and Majkrzak C F 1994 *Phys. Rev.* B **49** 11967
[43] Altarelli M, Núñez-Regueiro M D and Papoular M 1995 *Phys. Rev. Lett.* **74** 3840
[44] Weinrib A and Halperin B I 1983 *Phys. Rev.* B **27** 413
[45] Palmer S B and Greenough R D 1976 *J. Magn. Magn. Mater.* **1** 310
[46] Van Doorn C F, Van Delden D C and Du Plessis P de V 1982 *J. Magn. Magn. Mater.* 27 124
[47] Du Plessis P de V, Brits G H F, Abelman H and Fawcett E 1988 *Mater. Sci. Forum* **27/28** 253
[48] Burger J P, Vajda P, Daou J N and Chouteau G 1986 *J. Phys. F: Met. Phys.* **16** 1275
[49] Venter A M, Du Plessis P de V, Eloff G A and Fawcett E 1990 *J. Phys.: Condens. Matter* **2** 1363
[50] Schofield P 1969 *Phys. Rev. Lett.* **22** 606
[51] Betsuyaku H 1979 *Phys. Rev. Lett.* **42** 536
[52] Bennett H S 1969 *Phys. Rev.* **185** 801
[53] Bennett H S 1969 *Phys. Rev.* **181** 978
[54] Bennett H S and Pytte E 1967 *Phys. Rev.* **155** 553
[55] Moran T J and Lüthi B 1969 *Phys. Lett.* **29A** 665
[56] Rhyne J J, Legvold S and Rodine E T 1967 *Phys. Rev.* **154** 266
[57] Tonnies J J, Gschneidner K A and Spedding F H 1971 *J. Appl. Phys.* **42** 3275
[58] Palmer S B 1970 *J. Phys. Chem. Solids* **31** 143
[59] Liebfried G and Ludwig W 1961 *Solid State Physics* vol 12, ed F Seitz and D Turnbull (New York: Academic) p 275
[60] *Landolt–Börnstein New Series* 1992 Group III, vol 29 a (Berlin: Springer)
[61] Walcott N M 1959 *J. Chem. Phys.* **31** 536
[62] Arrott A, Werner S A and Kendrick H 1965 *Phys. Rev. Lett.* **14** 1022 and references cited therein
[63] Tang C C, Haycock P W, Stirling W G, Wilson C C, Keen D and Fort D 1995 *Physica* B **205** 105
[64] Aharony A and Fisher M E 1973 *Phys. Rev* B **8** 3323
[65] Aharony A 1973 *Phys. Rev.* B **8** 3342
[66] Aharony A 1973 *Phys. Rev.* B **8** 3349
[67] Aharony A 1973 *Phys. Rev.* B **8** 3358
[68] Stanley H E 1971 *Introduction to Phase Transitions and Critical Phenomena* (Oxford: Clarendon)